Structural and Multidisciplinary Optimization (2020) 62:1535–1546
https://doi.org/10.1007/s00158-020-02560-0

INDUSTRIAL APPLICATION PAPER

Shape optimization of running shoes with desired deformation properties

Mai Nonogawa[1] · **Kenzen Takeuchi**[2] · **Hideyuki Azegami**[3]

Received: 31 October 2019 / Revised: 26 February 2020 / Accepted: 27 February 2020 / Published online: 18 April 2020

Abstract

The present paper describes a shape optimization procedure for designing running shoes, focusing on two mechanical properties, namely, the shock absorption and the stability keeping the right posture. These properties are evaluated from two deformations of a sole at characteristic timings during running motion. We define approximate planes for the deformations of sole's upper boundary by least squares method. Using the planes, we choose the tilt angle in the shoe width direction at the mid stance phase of running motion as an objective function representing the stability, and the sunk amount at the contact phase of running motion as a constraint function representing the shock absorption. We assume that the sole is a bonded structure of soft and hard hyper-elastic materials, and the bonding and side boundaries are variable. In this study, we apply the formulation of nonparametric shape optimization to the sole considering finite deformation and contact condition of the bottom of the sole with the ground. Shape derivatives of the cost (objective and constraint) functions are obtained using the adjoint method. The H^1 gradient method using these shape derivatives is applied as an iterative algorithm. To solve this optimization problem, we developed a computer program combined with some commercial softwares. The validity of the optimization method is confirmed by numerical examples.

Keywords Running shoes · Hyper-elastic material · Shape optimization · Boundary value problem · H^1 gradient method

1 Introduction

Running is one of the most popular sports in the world. However, it has been reported that the risk of injuries to lower extremities is greater than other sports, because repeated loads are applied to lower extremities during running (Matheson et al. 1987). For this reason, running shoes should not only enhance the runner's performance but also prevent injuries during running.

Shoes have various requirement properties, such as cushioning property, shoe stability, grip property, and breathability (Cavanagh 1980; Nishiwaki 2008). Especially in the procedure designing sole of shoes, we often focus on the cushioning property and the shoe stability. The cushioning property means absorption of the impact from the ground at the contact phase. It is evaluated using time derivative of vertical ground reaction force (for instance Gard and Konz (2004), Clarke et al. (1983), Nigg et al. (1987, 1988), and Nigg (1980)). Meanwhile, the shoe stability means suppression of excessive foot joint motions called as pronation at the mid stance phase. It is evaluated using the angle between heel and lower extremity (for instance Nigg (1980), Woensel and Cavanagh (1992), Areblad et al. (1990), and Stacoff et al. (1992)). A sole that is made of soft material has good cushioning property but may not have good shoe stability. In the case of hard material, the contrary may be true.

Apparently, the sole which consists of only one material cannot provide both good properties. Some sole designs combining different hardness materials to improve both properties were reported (Nakabe and Nishiwaki 2002; Oriwol et al. 2011). These soles have a part made of hard material on the inside from the heel to the mid foot to

Responsible Editor: Seonho Cho

✉ Mai Nonogawa
mai.nonogawa@asics.com

[1] Institute of Sports Science, Asics Corporation, 6-2-1, Takatsukadai, Nishiku, Kobe 651-2271, Japan

[2] Faculty of Engineering and Design, Kagawa University, 1-1, Saiwai-cho, Takamatsu, 760-8521, Japan

[3] Graduate School of Informatics, Nagoya University, Furo-cho, Chikusa-ku, Nagoya 464-8601, Japan

increase rigidity of the sole. The hard part can prevent the heel to tilt towards the heel's region and improve the stability, while it may reduce cushioning property. However, the shape of the hard material in the heel was rectangular. We have not found any cases in which both the shoe stability and the cushioning property are improved by designing the shape of the material boundary using optimization method.

Some nonlinearities must be considered to predict mechanical properties of running shoes. It is expected that 20% or more of strain occurs in the sole during running since the ground reaction force in the vertical direction is two to three times of runner's weight (Gard and Konz 2004; Clarke et al. 1983, Nigg et al. 1987, 1988, Nigg 1980). Because of this, one has to consider geometrical nonlinearity in predicting mechanical properties of running shoes. The soles of running shoes should therefore be made of multiple materials with strong nonlinearity such as resin foams, resins, and rubbers to satisfy the various required properties. For example, it is known that resin foams have complicated behaviors under compressive load (Gibson and Ashby 1980; Mills 2007) and must be modeled as some hyper-elastic materials. In addition to this, contact condition must be taken into account because the bottom surface of the sole contacts with the ground at different parts from the moment of the first contact until complete separation from ground.

Many methods of analyzing design sensitivity of nonlinear problems have been researched over the years and applied to a variety of design optimization problems (Kaneko and Majer 1981; Ryu et al. 1985; Cardoso and Arora 1988; Tsay and Arora 1990; Vidal et al. 1991; Vidal and Haber 1993; Hisada 1995; Yamazaki and Shibuya 1998; Yuge and Kikuchi 1995). However, these methods were applicable only to parametric or sizing optimization problems. Focusing on nonparametric shape optimization methods, Ihara et al. (1999) solved a shape optimization problem minimizing the external work of an elasto-plastic body. They evaluated the shape derivative of the cost function by the adjoint method and obtained the search vector of domain variation by the traction method (Azegami and Wu 1996; Azegami and Takeuchi 2006) (H^1 gradient method for domain variation (Azegami 2016, 2017). Kim et al. (2000) presented a sensitivity analysis for shape optimization problems considering the infinitesimal elasto-plasticity with a frictional contact condition. In their work, the direct differentiation method was used to compute the displacement sensitivity, and the sensitivities of various performance measures were computed from the displacement sensitivity. In updating the shape, the authors used the so-called isoparametric mapping method (Choi and Chang 1994). Furthermore, Tanaka and Noguchi (2004) presented a shape optimization method similar to the traction method but described by a discrete form, and applied to structural designs with strong nonlinearity such as a flexible micromanipulator made of hyper-elastic material. Meanwhile, Iwai et al. (2010) presented a numerical solution to shape optimization problems of contacting elastic bodies for controlling contact pressure. They used an error norm of the contact pressure to a desired distribution as an objective cost function and evaluated its shape derivative by the adjoint method and reshaped by the traction method. In these aforementioned works, the studies conducted focus on basic problems, though they include geometrical and material nonlinearities.

In this study, we propose a shape optimization method with respect to the desired shoe stability and cushioning property for soles of running shoes. We define the indices to evaluate both properties and then formulate a shape optimization problem using the indices as cost functions. The shape derivatives of cost functions are derived theoretically. Using the shape derivatives, shape optimization can be performed based on the standard procedure of H^1 gradient method (Azegami 2016).

In the following sections, we use the notation $W^{s,\bar{p}}(\Omega;\mathbb{R})$ to represent the Sobolev space for the set of functions defined in Ω that corresponds to a value of $\mathbb{R}$ and is $s \in [0,\infty]$ times differentiable and $\bar{p} \in [1,\infty]$-th-order Lebesgue integrable. Furthermore, $L^{\bar{p}}(\Omega;\mathbb{R})$ and $H^s(\Omega;\mathbb{R})$ are denoted by $W^{0,\bar{p}}(\Omega;\mathbb{R})$ and $W^{s,2}(\Omega;\mathbb{R})$, respectively. In addition, the notation $C^{0,\sigma}(\Omega;\mathbb{R})$ is used to represent the Hölder space with a Hölder index $\sigma \in (0,1]$. In particular, $C^{0,1}(\Omega;\mathbb{R})$ is called the Lipschitz space. With respect to a reflexive Sobolev space X, we denote its dual space by X' and the dual product of $(x,y) \in X \times X'$ by $\langle x,y\rangle$. Specifically, $f'(\boldsymbol{x})[\boldsymbol{y}]$ represents the Fréchet derivative $\langle f'(\boldsymbol{x}),\boldsymbol{y}\rangle$ of $f : X \to \mathbb{R}$ at $\boldsymbol{x} \in X$ with respect to an arbitrary variation $\boldsymbol{y} \in X$. Additionally, $f_{\boldsymbol{x}}(\boldsymbol{x},\boldsymbol{y})[\boldsymbol{z}]$ represents the Fréchet partial derivative. The notation $\forall$ means the word "for all", and $\boldsymbol{A}\cdot\boldsymbol{B}$ represents the scalar product $\sum_{(i,j)\in\{1,\ldots,m\}^2} a_{ij}b_{ij}$ with respect to $\boldsymbol{A} = (a_{ij})_{ij}$, $\boldsymbol{B} = (b_{ij})_{ij} \in \mathbb{R}^{m\times m}$.

2 Sole model

Let us consider a conceptual sole model as depicted in Fig. 1. We assume that a sole of running shoes is composed of multiple hyper-elastic bodies and contacts with the ground. In this paper, Ω_{10} and Ω_{20} denote three-dimensional bounded open domains of hyper-elastic bodies initially made of soft and hard materials for the sole, Ω_{30} represents a domain of hyper-elastic body for the ground, and those that do not overlap with each other. Let Ω_0 denote $\bigcup_{i\in\{1,2,3\}}\Omega_{i0}$. The domains in Fig. 1 deformed by a domain variation, which mapping is denoted as $\boldsymbol{i}+\boldsymbol{\phi} : \Omega_0 \to \Omega(\boldsymbol{\phi}) = \bigcup_{i\in\{1,2,3\}}\Omega_i(\boldsymbol{\phi})$ ($\boldsymbol{i}$ is the identity mapping), and

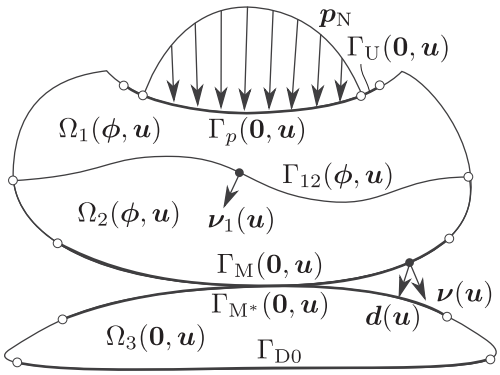

Fig. 1 A conceptual sole model

by finite hyper-elastic deformation generated by the map $\boldsymbol{i}+\boldsymbol{u}:\Omega(\boldsymbol{\phi})=\Omega(\boldsymbol{\phi},\mathbf{0})\to\Omega(\boldsymbol{\phi},\boldsymbol{u})=\bigcup_{i\in\{1,2,3\}}\Omega_i(\boldsymbol{\phi},\boldsymbol{u})$. The precise definitions will be introduced below.

2.1 Initial domains and boundary conditions

For the initial domains, we assume that the boundaries $\partial\Omega_{i0}$ ($i\in\{1,2,3\}$) of Ω_{i0} are at least Lipschitz continuous. The domains Ω_{10} and Ω_{20} are bonded on the boundary $\Gamma_{120}=\partial\Omega_{10}\cap\partial\Omega_{20}$. The domains Ω_{20} and Ω_{30} are joined by the boundary $\Gamma_{\mathrm{M0}}\cap\Gamma_{\mathrm{M}^*0}$, where Γ_{M0} and Γ_{M^*0} denote master and slave boundaries having possibility to contact on $\partial\Omega_{20}\setminus\bar{\Gamma}_{120}$ and $\partial\Omega_{30}$, respectively. The boundary Γ_{D0} on $\partial\Omega_{30}\setminus\bar{\Gamma}_{\mathrm{M}^*0}$ is a Dirichlet boundary on which the hyper-elastic deformation is fixed. We use the notation $\Gamma_{\mathrm{N0}}=\bigcup_{i\in\{1,2,3\}}\partial\Omega_{i0}\setminus\left(\bar{\Gamma}_{\mathrm{D0}}\cup\bar{\Gamma}_{120}\right)$ for a Neumann boundary and assume that a traction force $\boldsymbol{p}_{\mathrm{N}}$ is applied on $\Gamma_{p0}\subset\partial\Omega_{10}\setminus\bar{\Gamma}_{120}\subset\Gamma_{\mathrm{N0}}$ and varies with the boundary measure during domain deformation, whose definition will be given later. Moreover, $\Gamma_{\mathrm{U0}}\subset\partial\Omega_{10}\setminus\bar{\Gamma}_{120}$, which includes Γ_{p0}, represents the boundary to observe the deformation of sole, which will be used to define cost functions.

2.2 Domain variations

In this study, we assume that Ω_0 is a variable domain. As previously stated, the varied domain is defined as

$$\Omega(\boldsymbol{\phi})=\{(\boldsymbol{i}+\boldsymbol{\phi})(\boldsymbol{x})\mid\boldsymbol{x}\in\Omega_0\},$$

where $\boldsymbol{\phi}$ represents the displacement in the domain variation. Similarly, with respect to an initial domain or boundary $(\cdot)_0$, $(\cdot)(\boldsymbol{\phi})$ represents $\{(\boldsymbol{i}+\boldsymbol{\phi})(\boldsymbol{x})\mid\boldsymbol{x}\in(\cdot)_0\}$.

When the design variable $\boldsymbol{\phi}$ is selected as above, the domain of the solution to a state determination problem (hyper-elastic deformation problem) varies with the domain variation. Such a situation makes it difficult to apply a general formulation of function optimization problem. Hence, we will expand the domain of $\boldsymbol{\phi}$ from Ω_0 to $\mathbb{R}^3$ and assume $\boldsymbol{\phi}:\mathbb{R}^3\to\mathbb{R}^3$. Furthermore, since we will be considering the gradient method on a Hilbert space later, a linear space and an admissible set for $\boldsymbol{\phi}$ are defined as

$$X=\left\{\boldsymbol{\phi}\in H^1\left(\mathbb{R}^3;\mathbb{R}^3\right)\;\middle|\;\boldsymbol{\phi}=\mathbf{0}\ \text{on}\ \Gamma_{\mathrm{C0}}=\Gamma_{\mathrm{D0}}\cup\Gamma_{\mathrm{U0}}\cup\Gamma_{\mathrm{M0}}\cup\Gamma_{\mathrm{M}^*0}\right\},\tag{1}$$

$$\mathcal{D}=X\cap C^{0,1}\left(\mathbb{R}^3;\mathbb{R}^3\right).\tag{2}$$

In the definition of X, the boundary conditions for domain variation were added from the situation of the present study. The additional condition for $\mathcal{D}$ was added to guarantee that $\Omega(\boldsymbol{\phi})$ has Lipschitz regularity.

3 Hyper-elastic deformation problem

In the shape optimization problem formulated later, the solution $\boldsymbol{u}:\Omega(\boldsymbol{\phi})\to\mathbb{R}^3$ of hyper-elastic deformation problem will be used in cost functions. In this section, we will formulate this problem according to a standard procedure for hyper-elastic continuum.

We define a linear space and an admissible set for $\boldsymbol{u}$ as

$$U=\left\{\boldsymbol{u}\in H^1\left(\mathbb{R}^3;\mathbb{R}^3\right)\;\middle|\;\boldsymbol{u}=\mathbf{0}\ \text{on}\ \Gamma_{\mathrm{D0}}\right\},\tag{3}$$

$$\mathcal{S}=U\cap W^{2,2q_{\mathrm{R}}}\left(\mathbb{R}^3;\mathbb{R}^3\right)\tag{4}$$

for $q_{\mathrm{R}}>3$. The additional condition for $\mathcal{S}$ was added to guarantee the domain variation obtained by the H^1 gradient method introduced later being in $\mathcal{D}$.

As explained in Section 2, we consider that the traction $\boldsymbol{p}_{\mathrm{N}}$ acting on Γ_{p0} deforms $\Omega(\boldsymbol{\phi})=\Omega(\boldsymbol{\phi},\mathbf{0})$ as

$$\Omega(\boldsymbol{\phi},\boldsymbol{u})=\{(\boldsymbol{i}+\boldsymbol{u})(\boldsymbol{x})\mid\boldsymbol{x}\in\Omega(\boldsymbol{\phi})\}.$$

Similarly, with respect to any other domain or boundary $(\cdot)(\boldsymbol{\phi})$, $\{(\boldsymbol{i}+\boldsymbol{u})(\boldsymbol{x})\mid\boldsymbol{x}\in(\cdot)(\boldsymbol{\phi})\}$ is denoted as $(\cdot)(\boldsymbol{\phi},\boldsymbol{u})$.

On the boundary Γ_{M0}, having the possibility to contact with Γ_{S0}, we define the shortest vector from $\boldsymbol{x}\in\Gamma_{\mathrm{M}}(\mathbf{0},\boldsymbol{u})$ to $\Gamma_{\mathrm{M}^*}(\mathbf{0},\boldsymbol{u})$ by $\boldsymbol{d}(\boldsymbol{u}):\Gamma_{\mathrm{M}}(\mathbf{0},\boldsymbol{u})\to\mathbb{R}^3$ and a penetration distance by

$$g(\boldsymbol{u})=-\boldsymbol{d}(\boldsymbol{u})\cdot\boldsymbol{\nu}(\boldsymbol{u})\quad\text{on}\ \Gamma_{\mathrm{M}}(\mathbf{0},\boldsymbol{u}),\tag{5}$$

where $\boldsymbol{\nu}(\boldsymbol{u})$ is the outward unit normal vector on $\Gamma_{\mathrm{M}}(\mathbf{0},\boldsymbol{u})$. We introduce a Lagrange multiplier $p:\Gamma_{\mathrm{M}}(\mathbf{0},\boldsymbol{u})\to\mathbb{R}$ to the nonpenetrating condition $g(\boldsymbol{u})\le 0$. The physical meaning of $p\ge 0$ is the absolute value of contact pressure. For p, a linear space and an admissible set are defined as

$$P=H^1\left(\mathbb{R}^3;\mathbb{R}\right),$$

$$\mathcal{Q}=P\cap W^{2,2q_{\mathrm{R}}}\left(\mathbb{R}^3;\mathbb{R}\right).$$

A strain used in hyper-elastic deformation problem is defined according to the standard procedure. With respect

to the mapping $\boldsymbol{y} = \boldsymbol{i} + \boldsymbol{u} : \Omega_0 \to \Omega$, let the deformation gradient tensor be

$$\boldsymbol{F}(\boldsymbol{u}) = \left(\frac{\partial y_i}{\partial x_i}\right)_{ij} = \left(\nabla \boldsymbol{y}^\top\right)^\top = \boldsymbol{I} + \left(\nabla \boldsymbol{u}^\top\right)^\top,$$

and the Green-Lagrange strain be

$$\begin{aligned}\boldsymbol{E}(\boldsymbol{u}) &= \left(\varepsilon_{ij}(\boldsymbol{u})\right)_{ij} = \frac{1}{2}\left(\boldsymbol{F}^\top(\boldsymbol{u})\,\boldsymbol{F}(\boldsymbol{u}) - \boldsymbol{I}\right)\\ &= \boldsymbol{E}_{\mathrm{L}}(\boldsymbol{u}) + \frac{1}{2}\boldsymbol{E}_{\mathrm{B}}(\boldsymbol{u},\boldsymbol{u}),\end{aligned}$$

where $\boldsymbol{I}$ denotes the third-order unit matrix. $\boldsymbol{E}_{\mathrm{L}}(\boldsymbol{u})$ and $\boldsymbol{E}_{\mathrm{B}}(\boldsymbol{u},\boldsymbol{v})$ are defined as

$$\begin{aligned}\boldsymbol{E}_{\mathrm{L}}(\boldsymbol{u}) &= \frac{1}{2}\left(\nabla \boldsymbol{u}^\top + \left(\nabla \boldsymbol{u}^\top\right)^\top\right),\\ \boldsymbol{E}_{\mathrm{B}}(\boldsymbol{u},\boldsymbol{v}) &= \frac{1}{2}\left(\nabla \boldsymbol{u}^\top\left(\nabla \boldsymbol{v}^\top\right)^\top + \nabla \boldsymbol{v}^\top\left(\nabla \boldsymbol{u}^\top\right)^\top\right).\end{aligned}$$

The definition of constitutive equation for hyper-elastic material is started by assuming the existence of a nonlinear elastic potential $\pi : \mathbb{R}^{3\times 3} \to \mathbb{R}$ which gives the second Piola-Kirchhoff stress tensor as

$$\boldsymbol{S}(\boldsymbol{u}) = \frac{\partial \pi(\boldsymbol{E}(\boldsymbol{u}))}{\partial \boldsymbol{E}(\boldsymbol{u})}.$$

In this paper, we will use the Neo-Hookean model and the hyper foam model (Dassault Systèmes 2018), in which π are given as

$$\pi(\boldsymbol{E}(\boldsymbol{u})) = e_1(i_1(\boldsymbol{u}) - 3) + \frac{1}{e_2}(i_3(\boldsymbol{u}) - 1)^2, \tag{6}$$

$$\begin{aligned}\pi(\boldsymbol{E}(\boldsymbol{u})) = \sum_{i\in\{1,\ldots,n_{\mathrm{H}}\}} \frac{2\mu_i}{k_i^2}\Big[&m_1^{k_i}(\boldsymbol{u}) + m_2^{k_i}(\boldsymbol{u})\\ &+ m_3^{k_i}(\boldsymbol{u}) - 3 + \frac{1}{l_i}\left(i_3^{-k_i l_i}(\boldsymbol{u}) - 1\right)\Big],\end{aligned} \tag{7}$$

respectively. Here, e_i, k_i, l_i, and μ_i denote material parameters. n_{H} represents the order for the hyper foam model. The first and third invariants $i_1(\boldsymbol{u})$ and $i_3(\boldsymbol{u})$ are defined by

$$\begin{aligned}i_1(\boldsymbol{u}) &= i_3^{-2/3}(\boldsymbol{u})\left(m_1^2(\boldsymbol{u}) + m_2^2(\boldsymbol{u}) + m_3^2(\boldsymbol{u})\right),\\ i_3(\boldsymbol{u}) &= \det \boldsymbol{F}(\boldsymbol{u}),\end{aligned}$$

where $m_1(\boldsymbol{u}), m_2(\boldsymbol{u})$, and $m_3(\boldsymbol{u})$ are the principal values of the right Cauchy-Green deformation tensor defined by

$$C(\boldsymbol{u}) = \boldsymbol{F}^\top(\boldsymbol{u})\,\boldsymbol{F}(\boldsymbol{u}) = 2\boldsymbol{E}(\boldsymbol{u}) + \boldsymbol{I}.$$

The first Piola-Kirchhoff stress $\boldsymbol{\Pi}(\boldsymbol{u})$ and Cauchy stress $\boldsymbol{\Sigma}(\boldsymbol{u})$ can be obtained by $\boldsymbol{S}(\boldsymbol{u})$ as

$$\boldsymbol{\Pi}(\boldsymbol{u}) = \boldsymbol{F}(\boldsymbol{u})\,\boldsymbol{S}(\boldsymbol{u}) = \omega(\boldsymbol{u})\,\boldsymbol{\Sigma}(\boldsymbol{u})\left(\boldsymbol{F}^{-1}(\boldsymbol{u})\right)^\top, \tag{8}$$

$$\boldsymbol{\Sigma}(\boldsymbol{u}) = \frac{1}{\omega(\boldsymbol{u})}\boldsymbol{F}(\boldsymbol{u})\,\boldsymbol{S}(\boldsymbol{u})\,\boldsymbol{F}^\top(\boldsymbol{u}), \tag{9}$$

where $\omega(\boldsymbol{u})$ represents $\det|\boldsymbol{F}(\boldsymbol{u})|$.

Based on the definitions above, we formulate the hyper-elastic deformation problem of a sole including contact as follows.

Problem 1 (Hyper-elastic deformation) For $\boldsymbol{\phi} \in \mathcal{D}$ and a given $\boldsymbol{p}_{\mathrm{N}}$ having proper regularity, find $(\boldsymbol{u}, p) \in \mathcal{S} \times \mathcal{Q}$ such that

$$-\nabla^\top \boldsymbol{\Pi}^\top(\boldsymbol{u}) = \boldsymbol{0}^\top \quad \text{in } \Omega(\boldsymbol{\phi}), \tag{10}$$

$$\boldsymbol{\Sigma}(\boldsymbol{u})\,\boldsymbol{\nu}(\boldsymbol{u}) = \boldsymbol{p}_{\mathrm{N}}(\boldsymbol{u}) \quad \text{on } \Gamma_p(\boldsymbol{0},\boldsymbol{u}), \tag{11}$$

$$\boldsymbol{\Sigma}(\boldsymbol{u})\,\boldsymbol{\nu}(\boldsymbol{u}) = \boldsymbol{0} \quad \text{on } \Gamma_{\mathrm{N}}(\boldsymbol{\phi},\boldsymbol{u}) \setminus \bar{\Gamma}_p(\boldsymbol{0},\boldsymbol{u}), \tag{12}$$

$$\boldsymbol{u} = \boldsymbol{0} \quad \text{on } \Gamma_{\mathrm{D0}}, \tag{13}$$

$$\boldsymbol{\Sigma}(\boldsymbol{u})\,\boldsymbol{\nu}(\boldsymbol{u}) = -p\boldsymbol{\nu}(\boldsymbol{u}) \quad \text{on } \Gamma_{\mathrm{M}}(\boldsymbol{0},\boldsymbol{u}) \cup \Gamma_{\mathrm{M}^*}(\boldsymbol{0},\boldsymbol{u}), \tag{14}$$

$$g(\boldsymbol{u}) \le 0, \quad p \ge 0, \quad pg(\boldsymbol{u}) = 0 \quad \text{on } \Gamma_{\mathrm{M}}(\boldsymbol{0},\boldsymbol{u}). \tag{15}$$

Equation (15) gives the KKT (Karush-Kuhn-Tucker) conditions for the contact on $\Gamma_{\mathrm{M}}(\boldsymbol{0},\boldsymbol{u})$. $\boldsymbol{p}_{\mathrm{N}}(\boldsymbol{u})$ in (11) is defined as varying with the boundary measure in a domain variation, which is defined by

$$\boldsymbol{p}_{\mathrm{N}}\,\mathrm{d}\gamma = \boldsymbol{p}_{\mathrm{N}}(\boldsymbol{u})\,\mathrm{d}\gamma(\boldsymbol{u}), \tag{16}$$

where $\mathrm{d}\gamma$ and $\mathrm{d}\gamma(\boldsymbol{u})$ denote the respective infinitesimal boundary measures before and after deformations.

For later use, we define the Lagrange function with respect to Problem 1 as

$$\begin{aligned}&\mathscr{L}_{\mathrm{P}}(\boldsymbol{u}, p, \boldsymbol{v})\\ &= -\int_{\Omega(\boldsymbol{\phi},\boldsymbol{u})} \boldsymbol{S}(\boldsymbol{u}) \cdot \boldsymbol{E}'(\boldsymbol{u})[\boldsymbol{v}]\,\mathrm{d}x\\ &\quad + \int_{\Gamma_p(\boldsymbol{0},\boldsymbol{u})} \boldsymbol{p}_{\mathrm{N}}(\boldsymbol{u}) \cdot \boldsymbol{v}(\boldsymbol{u})\,\mathrm{d}\gamma(\boldsymbol{u})\\ &\quad + \int_{\Gamma_{12}(\boldsymbol{\phi},\boldsymbol{0})} \Big[\boldsymbol{u}_1 \cdot \left\{\left(\boldsymbol{\Pi}'(\boldsymbol{u}_1)[\boldsymbol{v}_1] + \boldsymbol{\Pi}'(\boldsymbol{u}_2)[\boldsymbol{v}_1]\right)\boldsymbol{v}_1\right\}\\ &\quad + \boldsymbol{v}_1 \cdot \left\{\left(\boldsymbol{\Pi}(\boldsymbol{u}_1) + \boldsymbol{\Pi}(\boldsymbol{u}_2)\right)\boldsymbol{v}_1\right\}\Big]\,\mathrm{d}\gamma\\ &\quad - \int_{\Gamma_{\mathrm{M}}(\boldsymbol{0},\boldsymbol{u})} p\boldsymbol{\nu}(\boldsymbol{u}) \cdot \left(\boldsymbol{v}_{\mathrm{M}}(\boldsymbol{u}) - \boldsymbol{v}_{\mathrm{M}^*}(\boldsymbol{u})\right)\mathrm{d}\gamma(\boldsymbol{u}).\end{aligned} \tag{17}$$

Here, $\boldsymbol{v} \in U$ was introduced as the Lagrange multiplier and $\boldsymbol{v}_1$ is the outward unit normal to Ω_{10} on $\Gamma_{12}(\boldsymbol{\phi},\boldsymbol{u})$ (see Fig. 1). To obtain (17), we multiplied (10) by $\boldsymbol{v}$, integrated it over $\Omega(\boldsymbol{\phi},\boldsymbol{0})$, and used (8) and the boundary conditions. In this process, the notations

$$\begin{aligned}\boldsymbol{E}'(\boldsymbol{u})[\boldsymbol{v}] &= \boldsymbol{E}_{\mathrm{L}}(\boldsymbol{v}) + \boldsymbol{E}_{\mathrm{B}}(\boldsymbol{u},\boldsymbol{v}) = \boldsymbol{E}'^\top(\boldsymbol{u})[\boldsymbol{v}],\\ \boldsymbol{\Pi}'(\boldsymbol{u})[\boldsymbol{v}] &= \boldsymbol{F}'[\boldsymbol{v}]\,\boldsymbol{S}(\boldsymbol{u}) + \boldsymbol{F}(\boldsymbol{u})\,\boldsymbol{S}'(\boldsymbol{u})[\boldsymbol{v}],\\ \boldsymbol{F}'[\boldsymbol{v}] &= \frac{\partial \boldsymbol{v}}{\partial \boldsymbol{x}^\top},\\ \boldsymbol{S}'(\boldsymbol{u})[\boldsymbol{v}] &= \boldsymbol{D}\boldsymbol{E}'(\boldsymbol{u})[\boldsymbol{v}] = \boldsymbol{S}'^\top(\boldsymbol{u})[\boldsymbol{v}],\end{aligned}$$

were used. The operator $\boldsymbol{E}'(\boldsymbol{u})[\boldsymbol{v}]$ denotes $\sum_{i\in\{1,2,3\}}(\partial \boldsymbol{E}/\partial u_i)\,v_i$. Moreover, $\boldsymbol{u}_i$ and $\boldsymbol{v}_i$ $(i \in \{1, 2, \mathrm{M}, \mathrm{M}^*\})$

denote the vectors $\boldsymbol{u}$ and $\boldsymbol{v}$ in $\Omega_i(\boldsymbol{\phi}, \boldsymbol{0})$ or on $\Gamma_i(\boldsymbol{0}, \boldsymbol{u})$, respectively. In the right-hand side of (17), the integral on the internal boundary $\Gamma_{12}(\boldsymbol{\phi}, \boldsymbol{0})$ was added to later evaluate the shape derivative on the boundary. Moreover, $g'(\boldsymbol{u})[\boldsymbol{v}_{\mathrm{M}}(\boldsymbol{u}) - \boldsymbol{v}_{\mathrm{M}^*}(\boldsymbol{u})] = \boldsymbol{v}(\boldsymbol{u}) \cdot (\boldsymbol{v}_{\mathrm{M}}(\boldsymbol{u}) - \boldsymbol{v}_{\mathrm{M}^*}(\boldsymbol{u}))$ was used in the last term. Using $\mathscr{L}_{\mathrm{P}}$, the weak form of Problem 1 can be written as

$$\mathscr{L}_{\mathrm{P}}(\boldsymbol{u}, p, \boldsymbol{v}) = 0 \quad \forall \boldsymbol{v} \in U, \tag{18}$$

combined with (15). This condition can be replaced by a variational inequality as follows. When $\Gamma_{\mathrm{M}}(\boldsymbol{0}, \boldsymbol{u})$ and $\Gamma_{\mathrm{M}^*}(\boldsymbol{0}, \boldsymbol{u})$ contact-impact one another, the conditions $p > 0$ and $g(\boldsymbol{u}) = 0$ hold. To satisfy the inequality $g(\boldsymbol{u}) \leq 0$, we require the condition

$$\begin{aligned} &g'(\boldsymbol{u})[\boldsymbol{v}_{\mathrm{M}}(\boldsymbol{u}) - \boldsymbol{v}_{\mathrm{M}^*}(\boldsymbol{u})] \\ &= \boldsymbol{v}(\boldsymbol{u}) \cdot (\boldsymbol{v}_{\mathrm{M}}(\boldsymbol{u}) - \boldsymbol{v}_{\mathrm{M}^*}(\boldsymbol{u})) \leq 0 \end{aligned}$$

to hold. Therefore, defining

$$U_{\mathrm{C}} = \{\boldsymbol{u} \in U \mid g(\boldsymbol{u}) \leq 0 \text{ on } \Gamma_{\mathrm{M}}(\boldsymbol{u})\}, \tag{19}$$

we can rewrite (18) combined with (15) to obtain the variational inequality given by

$$\begin{aligned} &\int_{\Omega(\boldsymbol{\phi}, \boldsymbol{u})} \boldsymbol{S}(\boldsymbol{u}) \cdot \boldsymbol{E}'(\boldsymbol{u})[\boldsymbol{v}] \, \mathrm{d}x \\ &- \int_{\Gamma_{12}(\boldsymbol{\phi}, \boldsymbol{0})} \left[\boldsymbol{u}_1 \cdot \left\{\left(\boldsymbol{\Pi}'(\boldsymbol{u}_1)[\boldsymbol{v}_1] + \boldsymbol{\Pi}'(\boldsymbol{u}_2)[\boldsymbol{v}_1]\right)\boldsymbol{v}_1\right\}\right. \\ &\left. + \boldsymbol{v}_1 \cdot \{(\boldsymbol{\Pi}(\boldsymbol{u}_1) + \boldsymbol{\Pi}(\boldsymbol{u}_2))\boldsymbol{v}_1\}\right] \mathrm{d}\gamma \\ \geq &\int_{\Gamma_p(\boldsymbol{0}, \boldsymbol{u})} \boldsymbol{p}_{\mathrm{N}}(\boldsymbol{u}) \cdot \boldsymbol{v}(\boldsymbol{u}) \, \mathrm{d}\gamma(\boldsymbol{u}) \quad \forall \boldsymbol{v} \in U_{\mathrm{C}}. \end{aligned} \tag{20}$$

4 Approximate planes for sole deformation

The objective of this paper is to improve the properties of cushioning and shoe stability. In this section, we define how to evaluate those properties. To do so, we introduce approximate planes of sole's deformations and show the way to calculate them.

4.1 Definition of approximate planes

Figure 2 shows a solemodel, coordinate system $(x_1, x_2, x_3) \in \mathbb{R}^3$, and one of the approximate planes of deformation at time t_r with cost functions f_r ($r \in \{\mathrm{S}, \mathrm{C}\}$) which will be defined later.

Before showing the definition of the planes, we will explain conventional methods to evaluate the shoe stability and cushioning property. Shoe stability is evaluated by the angle between the heel and lower extremity or between the heel and the ground at the time of minimum of ground reaction force in the foot length direction. Cushioning property, on the other hand, is evaluated using the derivative

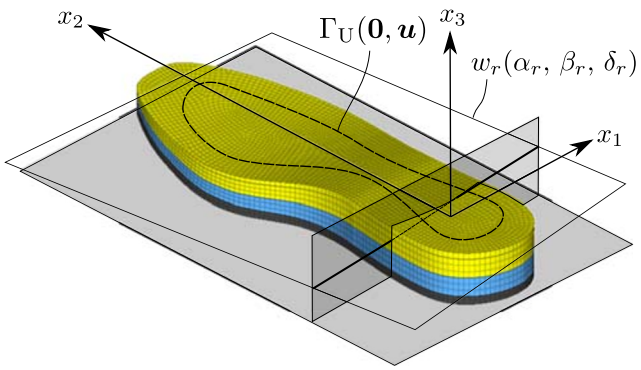

(a) Perspective view

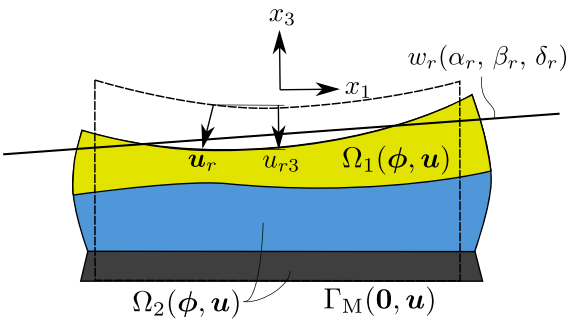

(b) Cross section in x_1–x_3 plane

Fig. 2 **a**, **b** The least squares planes w_r of displacement at t_r ($r \in \{\mathrm{S}, \mathrm{C}\}$)

of the vertical ground reaction force at the time of the first peak of vertical ground reaction force. According to experimental researches, it is thought that these values depend on the deformation of the sole. In particular, the displacement in x_3-direction on top surface of the sole is dominant.

Based on experience and information, we propose to evaluate the cushioning property and shoe stability using the parameters of the least squares approximate planes of the displacements in x_3-direction at characteristic timings during running motion.

The foot pressure distribution on each timing is measured experimentally using F-Scan (Tekscan, Inc.). The results are shown in Fig. 3. Among them, we use the pressure distributions at the times t_{S} (Fig. 3c) and t_{C} (Fig. 3a) for shoe stability and cushioning property, respectively, for $\boldsymbol{p}_{\mathrm{N}}$ in the static deformation problem (Problem 1). Appropriate contact condition between the bottom surface $\Gamma_{\mathrm{M}}(\boldsymbol{0}, \boldsymbol{u})$ of the sole and the ground $\Gamma_{\mathrm{M}^*}(\boldsymbol{0}, \boldsymbol{u})$ is considered at each time. We will write the two displacements obtained as the solutions of Problem 1 as $\boldsymbol{u}_r$ ($r \in \{\mathrm{S}, \mathrm{C}\}$) and components in x_3-direction as u_{r3}.

We define the least squares approximate plane of u_{r3} at each time by

$$w_r(\alpha_r, \beta_r, \delta_r) = \alpha_r x_1 + \beta_r x_2 + \delta_r, \tag{21}$$

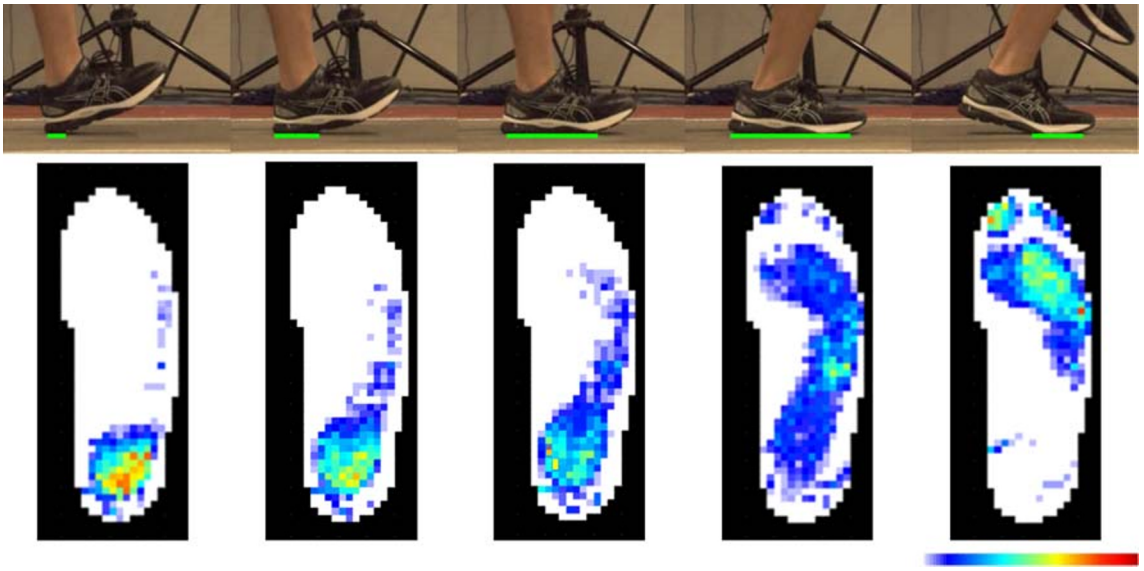

(a) Time t_C (b) (c) Time t_S (d) (e)

Fig. 3 **a**–**e** Running motion (upper) and pressure distributions (lower) measured on the top surface of sole

for $(x_1, x_2) \in \mathbb{R}^2$. Here, α_r, β_r, and δ_r are constants to express the gradients in x_1- and x_2-directions and the average of sinking in x_3-direction of the approximate plane of u_{r3}, respectively. Those parameters are functions of $\boldsymbol{u}_r$. So, we express them as $\alpha_r(\boldsymbol{u}_r)$, $\beta_r(\boldsymbol{u}_r)$, and $\delta_r(\boldsymbol{u}_r)$, respectively.

In this study, we will use $\alpha_S(\boldsymbol{u}_S)$ and $\delta_C(\boldsymbol{u}_C)$ for cost functions with respect to shoe stability and cushioning property, respectively.

4.2 Calculation of approximate planes

The parameters α_r, β_r, and δ_r can be obtained as a solution of a least square problem between u_{r3} and w_r. Here, the r is omitted for simplicity. We define the objective function for this problem as

$$\begin{aligned} f_U(\alpha,\beta,\delta) &= \int_{\Gamma_{U0}} (u_3 - w(\alpha,\beta,\delta))^2 \,\mathrm{d}\gamma \\ &= \int_{\Gamma_{U0}} \Big\{ u_3^2 + \alpha^2 x_1^2 + \beta^2 x_2^2 + \delta^2 \\ &\quad -2u_3(\alpha x_1 + \beta x_2 + \delta) \\ &\quad +2\alpha x_1 \beta x_2 + 2c\alpha x_1 + 2\delta\beta x_2 \Big\} \,\mathrm{d}\gamma, \end{aligned} \tag{22}$$

where $\Gamma_U(\mathbf{0}, \boldsymbol{u})$ is the boundary to observe sole deformation (refer to Figs. 1 and 2). The least square problem can then be written as follows.

Problem 2 (**Approximate plane**) For a given u_3, find α, β and δ satisfying

$$\min_{(\alpha,\beta,\delta)\in\mathbb{R}^3} f_U(\alpha,\beta,\delta).$$

Using the stationary conditions with partial differentiations of f_S by those parameters, the solution of Problem 2 can be obtained as

$$\begin{aligned} \alpha &= \int_{\Gamma_{U0}} x_1(u_3 - \beta x_2 - \delta)\,\mathrm{d}\gamma \Big/ \int_{\Gamma_{U0}} x_1^2 \,\mathrm{d}\gamma, \\ \beta &= \int_{\Gamma_{U0}} x_2(u_3 - \alpha x_1 - \delta)\,\mathrm{d}\gamma \Big/ \int_{\Gamma_{U0}} x_2^2 \,\mathrm{d}\gamma, \\ \delta &= \int_{\Gamma_{U0}} (u_3 - \alpha x_1 - \beta x_2)\,\mathrm{d}\gamma \Big/ \int_{\Gamma_{U0}} \mathrm{d}\gamma. \end{aligned}$$

Solving the above system of equations, the parameters α, β, and δ of the least squares planes can be expressed as

$$\begin{aligned} \alpha &= \frac{1}{\gamma}\Big\{ \left(c_0c_{22} - c_2^2\right) \int_{\Gamma_{U0}} x_1u_3 \,\mathrm{d}\gamma \\ &\quad + (c_1c_2 - c_0c_{12}) \int_{\Gamma_{U0}} x_2u_3 \,\mathrm{d}\gamma \\ &\quad + (c_2c_{12} - c_1c_{22}) \int_{\Gamma_{U0}} u_3 \,\mathrm{d}\gamma \Big\} \\ &= \sum_{j\in\{0,1,2\}} \bar{a}_j h_j(\boldsymbol{u}), \end{aligned} \tag{23}$$

$$\begin{aligned} \beta &= \frac{1}{\gamma}\Big\{ (c_1c_2 - c_0c_{12}) \int_{\Gamma_{U0}} x_1u_3 \,\mathrm{d}\gamma \\ &\quad + \left(c_0c_{11} - c_1^2\right) \int_{\Gamma_{U0}} x_2u_3 \,\mathrm{d}\gamma \\ &\quad + (c_1c_{12} - c_2c_{11}) \int_{\Gamma_{U0}} u_3 \,\mathrm{d}\gamma \Big\} \\ &= \sum_{j\in\{0,1,2\}} \bar{b}_j h_j(\boldsymbol{u}), \end{aligned} \tag{24}$$

$$\begin{aligned}\delta &= \frac{1}{\gamma}\left\{(c_2c_{12}-c_1c_{22})\int_{\Gamma_{\mathrm{U}0}} x_1u_3\,\mathrm{d}\gamma\right.\\ &\quad +(c_1c_{12}-c_2c_{11})\int_{\Gamma_{\mathrm{U}0}} x_2u_3\,\mathrm{d}\gamma\\ &\quad \left.+\left(c_{11}c_{22}-c_{12}^2\right)\int_{\Gamma_{\mathrm{U}0}} u_3\,\mathrm{d}\gamma\right\}\\ &= \sum_{j\in\{0,1,2\}} \bar{d}_j h_j(\boldsymbol{u}), \end{aligned} \tag{25}$$

where

$$\begin{aligned} c_0 &= \int_{\Gamma_{\mathrm{U}0}} \mathrm{d}\gamma, \quad c_1 = \int_{\Gamma_{\mathrm{U}0}} x_1\,\mathrm{d}\gamma,\\ c_2 &= \int_{\Gamma_{\mathrm{U}0}} x_2\,\mathrm{d}\gamma, \quad c_{11} = \int_{\Gamma_{\mathrm{U}0}} x_1^2\,\mathrm{d}\gamma,\\ c_{22} &= \int_{\Gamma_{\mathrm{U}0}} x_2^2\,\mathrm{d}\gamma, \quad c_{12} = \int_{\Gamma_{\mathrm{U}0}} x_1x_2\,\mathrm{d}\gamma,\\ \gamma &= c_0c_{11}c_{22}+2c_1c_2c_{12}-c_1^2c_{22}-c_2^2c_{11}-c_0c_{12}^2 \end{aligned}$$

and

$$\begin{aligned} h_0(\boldsymbol{u}) &= \int_{\Gamma_{\mathrm{U}0}} u_3\,\mathrm{d}\gamma,\\ h_1(\boldsymbol{u}) &= \int_{\Gamma_{\mathrm{U}0}} x_1u_3\,\mathrm{d}\gamma,\\ h_2(\boldsymbol{u}) &= \int_{\Gamma_{\mathrm{U}0}} x_2u_3\,\mathrm{d}\gamma. \end{aligned}$$

From here, we will denote α, β, and δ of (23), (24), and (25) at time t_r ($r \in \{\mathrm{S},\mathrm{C}\}$) by $\alpha(\boldsymbol{u}_r)$, $\beta(\boldsymbol{u}_r)$, and $\delta(\boldsymbol{u}_r)$, respectively.

5 Shape optimization problem

Using the definitions given in the previous section, we will now formulate the shape optimization problem that we will examine in this section. Considering the design process of shoes, we assume that there is an ideal value δ_{I} for the cushioning property $\delta(\boldsymbol{u}_{\mathrm{C}})$. Therefore, we define the objective and constraint cost functions as

$$f_{\mathrm{S}}(\boldsymbol{u}_{\mathrm{S}}) = \alpha(\boldsymbol{u}_{\mathrm{S}}), \tag{26}$$

$$f_{\mathrm{C}}(\boldsymbol{u}_{\mathrm{C}}) = \delta(\boldsymbol{u}_{\mathrm{C}}) - \delta_{\mathrm{I}}, \tag{27}$$

respectively. Using these cost functions, we construct a shape optimization problem as follows.

Problem 3 (Shape optimization) For f_{S} and f_{C} of (26) and (27), respectively, find $\Omega(\boldsymbol{\phi})$ such that

$$\min_{(\boldsymbol{\phi},\boldsymbol{u}_{\mathrm{S}},\boldsymbol{u}_{\mathrm{C}})\in\mathcal{D}\times\mathcal{S}^2} \{f_{\mathrm{S}}(\boldsymbol{u}_{\mathrm{S}}) \mid f_{\mathrm{C}}(\boldsymbol{u}_{\mathrm{C}}) = 0, \boldsymbol{u}_r (r\in\{\mathrm{S},\mathrm{C}\}) \text{ is the solution of Problem 1, } \alpha(\boldsymbol{u}_r), \beta(\boldsymbol{u}_r), \text{ and } \delta(\boldsymbol{u}_r) \text{ are calculated by (23), (24), and(25)}\}.$$

6 Shape derivatives of cost functions

In order to solve the shape optimization problem by a gradient-based method, the Fréchet derivatives of the cost functions with respect to variation of the design variable are required. We will derive them with the Lagrange multiplier method (the adjoint method). Using the Lagrange function $\mathscr{L}_{\mathrm{P}}$ with respect to Problem 1 defined in (17), the Lagrange function of f_r ($r \in \{\mathrm{S},\mathrm{C}\}$) can be defined as

$$\mathscr{L}_r(\boldsymbol{\phi},\boldsymbol{u}_r,p_r,\boldsymbol{v}_r) = f_r(\boldsymbol{u}_r) + \mathscr{L}_{\mathrm{P}}(\boldsymbol{\phi},\boldsymbol{u}_r,p_r,\boldsymbol{v}_r),$$

where $\boldsymbol{v}_r$ was introduced as the Lagrange multiplier with respect to Problem 1 for f_r. In the Lagrange multiplier method, the shape derivative (Fréchet derivative with respect to domain variation) of f_r is given by $\tilde{f}_r'(\boldsymbol{\phi})[\boldsymbol{\varphi}]$ using the notation $\tilde{f}_r(\boldsymbol{\phi}) = f_r(\boldsymbol{u}_r(\boldsymbol{\phi}))$, which is referred to as the reduced cost function, and calculated via the functional $\mathscr{L}_{r\boldsymbol{\phi}}(\boldsymbol{\phi},\boldsymbol{u}_r,p_r,\boldsymbol{v}_r)[\boldsymbol{\varphi}]$.

The shape derivative of $\mathscr{L}_r$ with respect to an arbitrary variation $(\boldsymbol{\varphi},\hat{\boldsymbol{u}},\hat{p},\hat{\boldsymbol{v}}) \in X\times U\times P\times U$ of $(\boldsymbol{\phi},\boldsymbol{u}_r,p_r,\boldsymbol{v}_r)$ can be written as

$$\begin{aligned}&\mathscr{L}_r'(\boldsymbol{\phi},\boldsymbol{u}_r,p_r,\boldsymbol{v}_r)[\boldsymbol{\varphi},\hat{\boldsymbol{u}},\hat{p},\hat{\boldsymbol{v}}]\\ &= \mathscr{L}_{r\boldsymbol{\phi}}(\boldsymbol{\phi},\boldsymbol{u}_r,p_r,\boldsymbol{v}_r)[\boldsymbol{\varphi}] + \mathscr{L}_{r\boldsymbol{u}_rp_r}(\boldsymbol{\phi},\boldsymbol{u}_r,p_r,\boldsymbol{v}_r)[\hat{\boldsymbol{u}},\hat{p}]\\ &\quad +\mathscr{L}_{r\boldsymbol{v}_r}(\boldsymbol{\phi},\boldsymbol{u}_r,p_r,\boldsymbol{v}_r)[\hat{\boldsymbol{v}}]. \end{aligned} \tag{28}$$

Here, the third term of the right-hand side of (28) becomes

$$\mathscr{L}_{r\boldsymbol{v}}(\boldsymbol{\phi},\boldsymbol{u}_r,p_r,\boldsymbol{v}_r)[\hat{\boldsymbol{v}}] = \mathscr{L}_{\mathrm{P}}(\boldsymbol{\phi},\boldsymbol{u}_r,p_r,\hat{\boldsymbol{v}}).$$

Then, if $(\boldsymbol{u}_r,p_r)$ is the solution of Problem 1, this term becomes zero. The second term of the right-hand side of (28) becomes

$$\begin{aligned}&\mathscr{L}_{r\boldsymbol{u}_rp_r}(\boldsymbol{\phi},\boldsymbol{u}_r,p_r,\boldsymbol{v}_r)[\hat{\boldsymbol{u}},\hat{p}]\\ &= -\int_{\Omega(\boldsymbol{\phi})} \left(\boldsymbol{S}'(\boldsymbol{u}_r)[\hat{\boldsymbol{u}}]\cdot\boldsymbol{E}'(\boldsymbol{u}_r)[\boldsymbol{v}_r]\right.\\ &\quad \left.+\boldsymbol{S}(\boldsymbol{u}_r)\cdot\boldsymbol{E}_{\mathrm{B}}(\hat{\boldsymbol{u}},\boldsymbol{v}_r)\right)\mathrm{d}x\\ &\quad -\int_{\Gamma_{\mathrm{M}+}(\boldsymbol{0},\boldsymbol{u}_r)} (\boldsymbol{v}_{r\mathrm{M}}(\boldsymbol{u}_r)-\boldsymbol{v}_{r\mathrm{M}^*}(\boldsymbol{u}_r))\\ &\quad \cdot\hat{p}\boldsymbol{\nu}(\boldsymbol{u}_r)\,\mathrm{d}\gamma(\boldsymbol{u}_r)\\ &\quad +\begin{cases}\sum_{j\in\{0,1,2\}}\bar{a}_jh_j(\hat{\boldsymbol{u}}) & (r=\mathrm{S})\\ \sum_{j\in\{0,1,2\}}\bar{d}_jh_j(\hat{\boldsymbol{u}}) & (r=\mathrm{C})\end{cases}, \end{aligned} \tag{29}$$

where we used the notation

$$\Gamma_{\mathrm{M}+}(\boldsymbol{0},\boldsymbol{u}_r) = \{\boldsymbol{x}\in\Gamma_{\mathrm{M}}(\boldsymbol{0},\boldsymbol{u}_r) \mid p(\boldsymbol{x})>0\},$$

and the coefficients a_j and d_j defined in (23) and (25). Noticing that $\mathscr{L}_{r\boldsymbol{u}_rp_r} = 0$, for an arbitrary $(\hat{\boldsymbol{u}},\hat{p}) \in U\times P$, is the weak form of the adjoint problem below, the second term on the right-hand side of (28) becomes zero when $\boldsymbol{v}_r$ is the solution of the following problem.

Problem 4 (**Adjoint problem for** f_r) Let $\boldsymbol{u}_r$ be the solution of Problem 1 for $\boldsymbol{\phi} \in \mathcal{D}$, find $\boldsymbol{v}_r \in \mathcal{S}$ such that

$$
\begin{aligned}
-\nabla^{\top} \boldsymbol{\Pi}'^{\top} (\boldsymbol{u}_r) [\boldsymbol{v}_r] &= \boldsymbol{0}^{\top} \quad \text{in } \Omega (\boldsymbol{\phi}), \\
\boldsymbol{\Pi}' (\boldsymbol{u}_r) [\boldsymbol{v}_r] \boldsymbol{v} &= \begin{cases} (\bar{a}_0 + \bar{a}_1 x_1 + \bar{a}_2 x_2) v_3 & (r = \mathrm{S}) \\ \left(\bar{d}_0 + \bar{d}_1 x_1 + \bar{d}_2 x_2\right) v_3 & (r = \mathrm{C}) \end{cases} \\
&\quad \text{on } \Gamma_{\mathrm{U}}, \\
\boldsymbol{\Pi}' (\boldsymbol{u}_r) [\boldsymbol{v}_r] \boldsymbol{v} &= \boldsymbol{0} \quad \text{on } \Gamma_{\mathrm{N}} (\boldsymbol{\phi}) \setminus \bar{\Gamma}_{\mathrm{U}}, \\
\boldsymbol{v}_r &= \boldsymbol{0} \quad \text{on } \Gamma_{\mathrm{D0}}, \\
\boldsymbol{v}_{\mathrm{M}} (\boldsymbol{u}_r) &= \boldsymbol{v}_{\mathrm{M}^*} (\boldsymbol{u}_r) \quad \text{on } \Gamma_{\mathrm{M}+} (\boldsymbol{0}, \boldsymbol{u}_r).
\end{aligned}
$$

If $(\boldsymbol{u}_r, p_r)$ and $\boldsymbol{v}_r$ are the solutions of Problem 1 and Problem 4, using the formula for shape derivative of $\mathscr{L}_r$ (see, for instance Delfour and Zolésio (2011, equations (4.7) and (4.16)), we obtain the shape derivative of $\tilde{f}_r (\boldsymbol{\phi})$ by

$$
\begin{aligned}
\tilde{f}_r' (\boldsymbol{\phi})[\boldsymbol{\varphi}] &= \mathscr{L}_{r\boldsymbol{\phi}} (\boldsymbol{\phi}, \boldsymbol{u}_r, p_r, \boldsymbol{v}_r) [\boldsymbol{\varphi}] = \langle \boldsymbol{g}_r, \boldsymbol{\varphi} \rangle \\
&= \int_{\partial\Omega(\boldsymbol{\phi}) \setminus \bar{\Gamma}_{\mathrm{C0}}} \boldsymbol{g}_{r\partial\Omega} \cdot \boldsymbol{\varphi} \, \mathrm{d}\gamma + \int_{\Gamma_{12}(\boldsymbol{\phi})} \boldsymbol{g}_{r12} \cdot \boldsymbol{\varphi} \, \mathrm{d}\gamma_1,
\end{aligned} \tag{30}
$$

where Γ_{C0} was defined in (1) and $\mathrm{d}\gamma_1$ denotes the infinitesimal boundary measure on $\partial\Omega_1 \left(\boldsymbol{\phi}, \boldsymbol{0}_{\mathbb{R}^3}\right)$. Here, the shape gradient for $\tilde{f}_r (\boldsymbol{\phi})$ ($r \in \{\mathrm{S}, \mathrm{C}\}$) is given by

$$
\boldsymbol{g}_{r\partial\Omega} = -\left(\boldsymbol{S} (\boldsymbol{u}_r) \cdot \boldsymbol{E}' (\boldsymbol{u}_r) [\boldsymbol{v}_r]\right) \boldsymbol{v}, \tag{31}
$$

$$
\begin{aligned}
\boldsymbol{g}_{r12} = \partial_{v_1} \big[& \boldsymbol{u}_{r1} \cdot \left\{ \left(\boldsymbol{\Pi}' (\boldsymbol{u}_{r1}) [\boldsymbol{v}_{r1}] + \boldsymbol{\Pi}' (\boldsymbol{u}_{r2}) [\boldsymbol{v}_{r1}] \right) \boldsymbol{v}_1 \right\} \\
& + \boldsymbol{v}_{r1} \cdot \left\{ \left(\boldsymbol{\Pi} (\boldsymbol{u}_{r1}) + \boldsymbol{\Pi} (\boldsymbol{u}_{r2}) \right) \boldsymbol{v}_{r1} \right\} \big] \boldsymbol{v}_1,
\end{aligned} \tag{32}
$$

where $\boldsymbol{v}_1$ denotes the outward unit normal on $\partial\Omega_1 (\boldsymbol{\phi}, \boldsymbol{0})$ and $\boldsymbol{u}_{ri}$ ($i \in \{1, 2\}$) and $\boldsymbol{v}_{r1}$ denote $\boldsymbol{u}_r$ and $\boldsymbol{v}_r$ on $\Omega_i (\boldsymbol{\phi}, \boldsymbol{0})$ and $\Omega_1 (\boldsymbol{\phi}, \boldsymbol{0})$, respectively. In the process to obtain the result of (28) with (29) and (30), the integrals defined over the boundary $\Gamma_{\mathrm{C0}} = \Gamma_{\mathrm{D0}} \cup \Gamma_{\mathrm{U0}} \cup \Gamma_{\mathrm{M0}} \cup \Gamma_{\mathrm{M}^*0}$ in (28) vanished since these boundaries are held fixed during domain deformation $\boldsymbol{\varphi} \in X$. Moreover, the terms including the mean curvature on $\Gamma_{12} \left(\boldsymbol{\phi}, \boldsymbol{0}_{\mathbb{R}^3}\right)$ also disappears due to the fact that the terms on $\partial\Omega_1 \left(\boldsymbol{\phi}, \boldsymbol{0}_{\mathbb{R}^3}\right)$ and $\partial\Omega_2 \left(\boldsymbol{\phi}, \boldsymbol{0}_{\mathbb{R}^3}\right)$ which have the unit normal vectors are oppositely directed.

7 Solution to shape optimization problem

Finally, we show the solution to the shape optimization problem given in Problem 3. Using the shape gradient $\boldsymbol{g}_r$ ($r \in \{\mathrm{S}, \mathrm{C}\}$) in (30), we can write the Lagrange function for Problem 3 and its shape derivative as

$$
\begin{aligned}
& \mathscr{L} (\boldsymbol{\phi}, \boldsymbol{u}_r, p_r, \boldsymbol{v}_r, \boldsymbol{v}_r; r \in \{\mathrm{S}, \mathrm{C}\}) \\
&= \mathscr{L}_{\mathrm{S}} (\boldsymbol{\phi}, \boldsymbol{u}_{\mathrm{S}}, p_{\mathrm{S}}, \boldsymbol{v}_{\mathrm{S}}) + \lambda_{\mathrm{C}} \mathscr{L}_{\mathrm{C}} (\boldsymbol{\phi}, \boldsymbol{u}_{\mathrm{C}}, p_{\mathrm{C}}, \boldsymbol{v}_{\mathrm{C}}),
\end{aligned} \tag{33}
$$

$$
\begin{aligned}
& \mathscr{L}_{\boldsymbol{\phi}} (\boldsymbol{\phi}, \boldsymbol{u}_r, p_r, \boldsymbol{v}_r, \boldsymbol{v}_r; r \in \{\mathrm{S}, \mathrm{C}\}) [\boldsymbol{\varphi}] \\
&= \langle \boldsymbol{g}_{\mathrm{S}}, \boldsymbol{\varphi} \rangle + \lambda_{\mathrm{C}} \langle \boldsymbol{g}_{\mathrm{C}}, \boldsymbol{\varphi} \rangle
\end{aligned} \tag{34}
$$

with respect to an arbitrary $\boldsymbol{\varphi} \in X$. Here, $\lambda_{\mathrm{C}} \in \mathbb{R}$ is the Lagrange multiplier for the constraint $f_{\mathrm{C}} (\boldsymbol{u}_{\mathrm{C}}) = 0$. The H^1 gradient method of domain variation type is formulated by seeking $\boldsymbol{\varphi}_{gr} \in X$ that decreases f_r with respect to iterations $k \in \{0, 1, \ldots\}$ by the following methods.

Problem 5 (H^1 **gradient method for** f_r) Let $a_X : X \times X \to \mathbb{R}$ be a bounded and coercive bilinear form in X, and c_a be a positive constant to control the magnitude of $\boldsymbol{\varphi}_{gr}$ ($r \in \{\mathrm{S}, \mathrm{C}\}$). For $\boldsymbol{g}_r \left(\boldsymbol{\phi}_k\right) \in X'$, find $\boldsymbol{\varphi}_{gr} \in X$ such that

$$
c_a a_X \left(\boldsymbol{\varphi}_{gr}, \boldsymbol{\psi}\right) = -\left\langle \boldsymbol{g}_r, \boldsymbol{\psi} \right\rangle \quad \forall \boldsymbol{\psi} \in X. \tag{35}
$$

In this paper, we use

$$
a_X (\boldsymbol{\varphi}, \boldsymbol{\psi}) = \int_{\Omega(\boldsymbol{\phi})} \left\{ \left(\nabla \boldsymbol{\varphi}^{\mathrm{T}}\right) \cdot \left(\nabla \boldsymbol{\psi}^{\mathrm{T}}\right) + c_{\Omega} \boldsymbol{\varphi} \cdot \boldsymbol{\psi} \right\} \mathrm{d}x,
$$

where c_{Ω} is a positive constant to guarantee the coerciveness of the bilinear form a_X. A simple algorithm for solving Problem 3 by the H^1 gradient method is shown next.

Algorithm 1 Shape optimization problem.

1. Set Ω_0, $\boldsymbol{\phi}_0 = \boldsymbol{i}$ (the identity mapping), c_a, c_{Ω} and $k = 0$.
2. Solve the state determination problems (Problem 1) for $r \in \{\mathrm{S}, \mathrm{C}\}$ at $\boldsymbol{\phi}_k$, and compute $f_{\mathrm{S}} (\boldsymbol{u}_{\mathrm{S}})$ and $f_{\mathrm{C}} (\boldsymbol{u}_{\mathrm{C}})$. Set $\delta_{\mathrm{I}} = f_{\mathrm{C}} (\boldsymbol{u}_{\mathrm{C}})$.
3. Solve the adjoint problems (Problem 4) for f_{S} and f_{C}, and calculate $\boldsymbol{g}_{\mathrm{S}}$ and $\boldsymbol{g}_{\mathrm{C}}$ at $\boldsymbol{\phi}_k$.
4. Use (35) to solve $\boldsymbol{\varphi}_{g\mathrm{S}}$ and $\boldsymbol{\varphi}_{g\mathrm{C}}$.
5. Calculate λ_1 by
$$
\lambda_{\mathrm{C}} = -\frac{f_{\mathrm{C}} (\boldsymbol{u}) + \langle \boldsymbol{g}_{\mathrm{C}}, \boldsymbol{\varphi}_{g\mathrm{S}} \rangle}{\langle \boldsymbol{g}_{\mathrm{C}}, \boldsymbol{\varphi}_{g\mathrm{C}} \rangle}. \tag{36}
$$
6. Compute $\boldsymbol{\varphi}_g$ using
$$
\boldsymbol{\varphi}_g = \boldsymbol{\varphi}_{g\mathrm{S}} + \lambda_{\mathrm{C}} \boldsymbol{\varphi}_{g\mathrm{C}}, \tag{37}
$$
set $\boldsymbol{\phi}_{k+1} = \boldsymbol{\phi}_k + \boldsymbol{\varphi}_g$, and compute $f_{\mathrm{S}} (\boldsymbol{u}_{\mathrm{S}})$ and $f_{\mathrm{C}} (\boldsymbol{u}_{\mathrm{C}})$.
7. Assess $\left| f_{\mathrm{S}} \left(\boldsymbol{u}_{\mathrm{S}} \left(\boldsymbol{\phi}_{k+1}\right)\right) - f_{\mathrm{S}} \left(\boldsymbol{u}_{\mathrm{S}} \left(\boldsymbol{\phi}_k\right)\right) \right| \leq \epsilon_0$.
   - If "Yes," proceed to 8.
   - If "No," replace $k + 1$ with k and return to 3.
8. Stop the algorithm.

We developed a computer program based on Algorithm 7. In the program, a commercial finite element program Abaqus 2018 (Dassault Systèmes) is used to solve state determination and adjoint problems (Problems 1 and 4). Moreover, OPTISHAPE-TS 2018 (Quint Corporation) is used to solve the boundary value problem (Problem 5) using the H^1 gradient method.

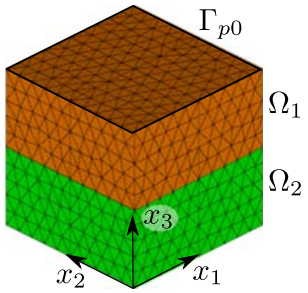

Fig. 4 A cubic model simplified sole

8 Numerical example

To confirm the solvability of the shape optimization problem (Problem 3) by the method shown in the previous section, we will show a numerical result using a cubic model. After that, a simple sole model will be used to demonstrate the validity of the presented method in the design of shoe sole such that the parameter for stability is maximized while the parameter for cushioning property keeps an ideal value.

In the following sections, we will show the necessity of considering the material nonlinearity in the analysis of the cubic model, as well as the necessity of using the contact condition in the case of a simple sole model.

8.1 Cubic model

Figure 4 shows a finite element model of a cubic body consisting of $\Omega_1 = (0, 0.05) \times (0, 0.05) \times (0.025, 0.05)$ [m^3] and $\Omega_2 = (0, 0.05) \times (0, 0.05) \times (0, 0.025)$ [m^3] defined in Fig. 1. The loading boundary Γ_{p0} is assumed on the upper boundary of Ω_1. The pressure distributions at the times t_S and t_C are assumed as follows:

$$\boldsymbol{p}_N = \begin{cases} -78\boldsymbol{e}_3[\text{kPa}] \text{ on } (0, 0.025) \times (0, 0.05) \times \{0.05\} \\ \boldsymbol{0}_{\mathbb{R}^3} \text{ on } (0.025, 0.05) \times (0, 0.05) \times \{0.05\} \end{cases}$$
at time t_S,

$$\boldsymbol{p}_N = \begin{cases} -78\boldsymbol{e}_3[kPa] \text{ on } (0, 0.05) \times (0.025, 0.05) \times \{0.05\} \\ \boldsymbol{0}_{\mathbb{R}^3} \text{ on } (0, 0.05) \times (0, 0.025) \times \{0.05\} \end{cases}$$
at time t_C,

where $\boldsymbol{e}_3$ denotes the unit vector on x_3-coordinate. The magnitude of the pressure is decided as much as equivalent to that of the actual pressure in the running motion. The material parameters used in ABAQUS are shown in Table 1 assuming that Ω_1 and Ω_2 are made of hyper foams. The Young's modulus e_Y used in the linear elastic analysis is calculated using the material parameters in Table 1 and Poisson's ratio ν_P by $2(1 + \nu_P)(\mu_1 + \mu_2 + \mu_3)$ ($e_Y = 0.78$ MPa and $\nu_P = 0.3$ in Ω_1, and $e_Y = 2.60$ MPa and $\nu_P = 0.3$ in Ω_2). The finite element model is constructed with 5304 ten-node tetrahedron elements and 8485 nodes. In this analysis, we assumed that $\Gamma_{M0} = \Gamma_{M^*0}$ is set as Γ_{D0} (i.e., fixed), and only the material boundary $\Gamma_{120} = \partial\Omega_{10} \cap \partial\Omega_{20}$ varies.

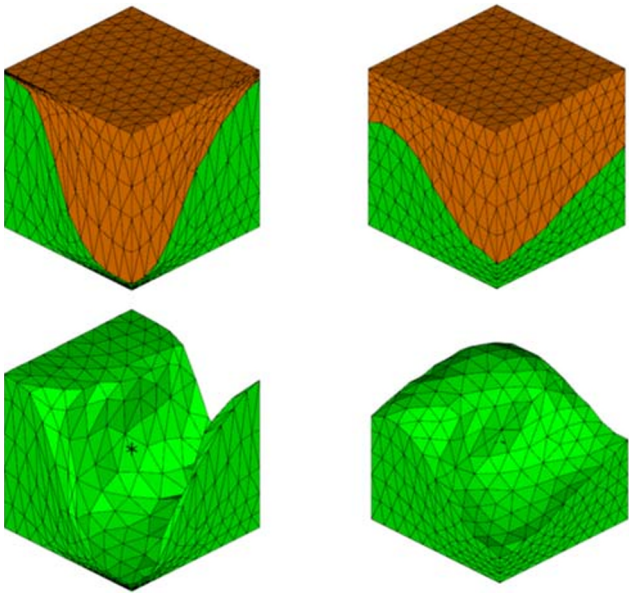

(a) Finite deformation with nonlinear material

(b) Small deformation with linear material

Fig. 5 **a**, **b** Optimized shapes of the cubic model

Figure 5 shows the optimized shapes of the cubic model. Figure 5a is the result obtained by considering the finite deformation and material nonlinearity, while (b) is the result obtained through linear elastic analysis. The iteration histories of cost functions are shown in Fig. 6. The notation $f_{S\,\text{init}}$ represents the value of f_S at the initial shape. From the graphs, it can be confirmed that both the objective cost functions f_S decreased monotonically while keeping the constraint condition $f_C \leq 0$. However, the amount of reduction is greater in the case considering the nonlinearities than the case of linear analysis. This result demonstrates that the linear analysis cannot follow the deformation sufficiently (too stiff) and cannot extend to the range of the deformation which we consider for the shoe design.

Table 1 Parameters of hyper foam used in the cubic model

Domain	μ_1 (MPa)	α_1 (-)	μ_2 (MPa)	α_2 (-)	μ_3 (MPa)	α_3 (-)	D_1 (-)	D_2 (-)	D_3 (-)
Ω_1	0.2142	19.9765	0.05814	17.4194	0.02720	−9.4883	0.3	0.3	0.3
Ω_2	0.7141	19.9765	0.1938	17.4194	0.0907	−9.4883	0.3	0.3	0.3

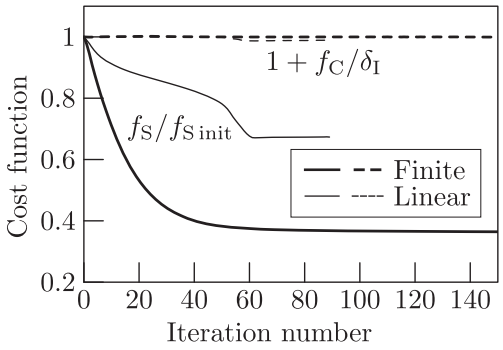

Fig. 6 Iteration history of cost functions in the cubic model

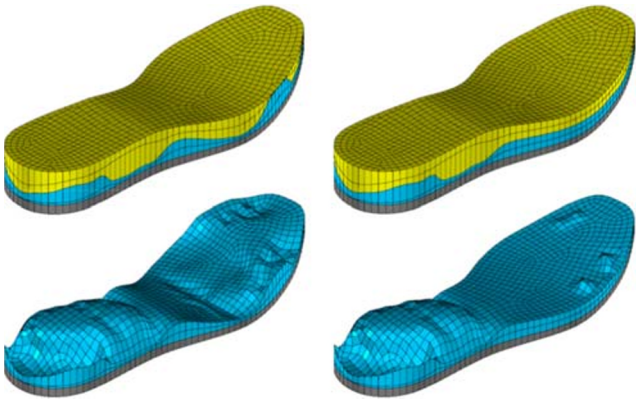

(a) Contact condition on the ground (b) Fixed condition with the ground

Fig. 7 **a**, **b** Optimized sole models considering finite deformation with nonlinear material

For reference, we examined a finite deformation analysis using the linear material. However, we could not continue the analysis by mesh distortion. In addition, using the optimized model obtained by the linear analysis shown in Fig. 5b, we analyzed the finite deformation with the nonlinear material and obtained the cost values $f_S/f_{S\,init} = 0.64$ and $1 + f_C/\delta_I = 1.03$. From the result, it can be confirmed that the inequality constraint $f_C \leq 0$ is violated. This violation is unacceptable in the design region of shoes.

8.2 Sole model

A finite element model of a sole is constructed with eight-node hexahedral elements as shown in Fig. 2. The model consists of three domains colored in yellow, light blue, and gray. The domains in yellow and light blue were modeled by hyper foam with different hardness. For the domain in gray, the Neo-Hookean model was used. We assumed that Ω_{20} consists of the domains in light blue and gray in which the gray domain is fixed in the domain variation. The parameters of these models were identified based on experimental results. We used the foot pressure distributions as shown in Fig. 3a and c for $\boldsymbol{p}_N$. In this analysis, we assumed that the ground Ω_{30} is a rigid body and fixed in the domain variation, and contact condition between the bottom surface $\Gamma_M(\mathbf{0}, \boldsymbol{u})$ of the sole and the ground $\Gamma_{M^*0} = \Gamma_{D0}$ with friction free is considered. For contact type in Abaqus 2018, the option 'surface-surface' was used. In the case using a fixed condition, we assumed that $\Gamma_{M0} = \Gamma_{M^*0}$ is the fixed boundary Γ_{D0}, and only the material boundary $\Gamma_{120} = \partial\Omega_{10} \cap \partial\Omega_{20}$ varies.

Figure 7a shows the optimized shapes of Ω_{10} and Ω_{20} obtained by the developed program using the nonlinear material and aforementioned contact condition. In contrast, Fig. 7b shows the result in which the contact condition is changed to the fixed condition on $\Gamma_{M0} = \Gamma_{M^*0} (= \Gamma_{D0})$. The iteration histories of cost functions with respect to the number of reshaping are shown in Fig. 8. Here, $f_{S\,init}$ denotes the f_S at the initial shape, too. From the graphs, it can be confirmed that the objective cost function f_S decreased monotonically while keeping the constraint condition $f_C \leq 0$. This variation means that maintaining the average sinking δ_I at the time t_C in the contact phase, the tilt angle α ($\boldsymbol{u}_S$) at the time t_S in the mid stance phase is minimized.

Comparing the results between the cases with contact condition and with fixed condition, we obtained a large reduction of f_S in the case with contact condition as evident in Fig. 8. A remarkable difference is found at the shape of mid top surface in $\Omega_2(\boldsymbol{\phi})$. In the contact case, a wavy variation in the thickness from the heel to toe is generated in the process of optimization, while only a small variation is created in the fixed case. Those differences can be considered as an effect of the contact and fixed conditions. When the contact condition is used with respect to the pressure distributions at the times t_S (Fig. 3c), the bottom surface of $\Omega_2(\boldsymbol{\phi})$ contacts with the mid foot from the heel and does not contact at the remaining part (Fig. 9b). This loading condition makes intensely focused variation in the mid top surface in $\Omega_2(\boldsymbol{\phi})$. On the other hand, when the fixed condition is used, all the bottom surface supports the pressure by tensile and compressible forces which are

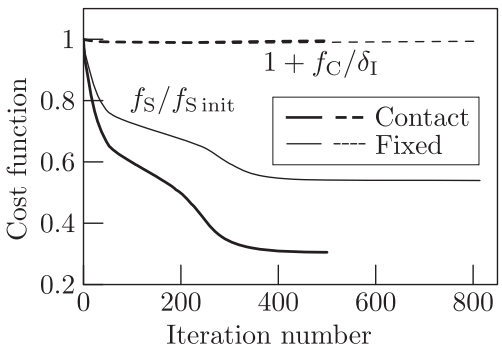

Fig. 8 Iteration history of cost functions in the sole model

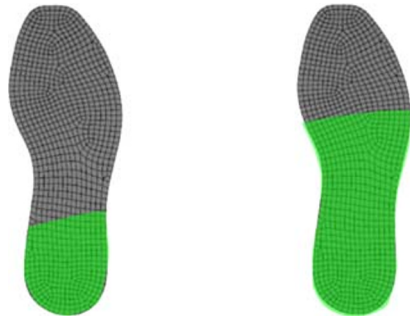

(a) Time t_C (b) Time t_S

Fig. 9 **a**, **b** Contacting regions

distributed widely. As a result, it can be considered that the shape variation becomes small and the reduction of f_S becomes small, too.

From the result that a great difference is observed between the contact and fixed conditions, it can be concluded that the contact condition is required in the design of sole.

9 Conclusion

In this paper, an optimized shape design problem for shoe sole improving the shoe stability and cushioning property was formulated using parameters of planes that approximate the deformations analyzed by the finite element method using the pressures measured during the running motion as external boundary forces. In the finite element analysis, finite deformation, nonlinear constitutive equations for hyper-elastic materials, and contact condition between the bottom of sole and the ground were taken into account. Using the approximate planes, the tilt angle in the mid stance phase and the average sinking in the contact phase were chosen as objective and constraint cost functions, respectively. The target boundaries to optimize were the bonded boundary of soft and hard materials and side boundary. Numerical results using a realistic finite element model demonstrated that the optimized shape of the formulated problem can be obtained by the presented method. Regarding the selection of the parameters for objective and constraint cost functions, we have to hear desires of running shoe developers based on evaluation by runners.

Compliance with ethical standards

Conflict of interest The authors declare that they have no conflict of interest.

Replication of results The results described in this paper can be replicated by implementing the formulas and algorithms described in this paper. Regarding the foot pressure distributions and material parameters for the sole model used in the numerical examples, the authors want to withhold its replication for commercial purposes.

References

Areblad M, Nigg BM, Ekstrand J, Olsson KO (1990) Three-dimensional measurement of rearfoot motion during running. J Biomech 23:933–940

Azegami H (2016) Shape optimization problems (in Japanese). Morikita Publishing, Tokyo

Azegami H (2017) Solution of shape optimization problem and its application to product design. In: Itou H, Kimura M, Chalupecký V, Ohtsuka K, Tagami D, Takada A (eds) Proceedings of the international conference CoMFoS15 Mathematical analysis of continuum mechanics and industrial applications, Springer Singapore, Mathematics for industry, 26: 83–98. https://doi.org/10.1007/978-981-10-2633-1

Azegami H, Takeuchi K (2006) A smoothing method for shape optimization: Traction method using the Robin condition. Int J Comput Methods 3(1):21–33

Azegami H, Wu ZQ (1996) Domain optimization analysis in linear elastic problems: Approach using traction method. JSME Int J Ser A 39(2):272–278

Cardoso JB, Arora JS (1988) Variational method for design sensitivity analysis in nonlinear structural mechanics. AIAA J 26:595–603

Cavanagh P (1980) The running shoe book. Anderson World, California

Choi KK, Chang KH (1994) A study on the velocity computation for shape design optimization. J Finite Elem Anal Des 15:317–347

Clarke TE, Frederick EC, Cooper LB (1983) Effects of running shoes on ground reaction forces. Int J Sports Med 4:247–251

Dassault Systèmes (2018) Abaqus Analysis User's Guide 2018. Vélizy-Villacoublay

Delfour MC, Zolésio JP (2011) Shapes and geometries: Metrics, analysis, differential calculus and optimization, 2nd edn. Society for Industrial and Applied Mathematics, Philadelphia

Gard SA, Konz RJ (2004) The effect of a shock-absorbing pylon on the gait of persons with unilateral transtibial amputation. J Rehabil Res Dev 40:109–124

Gibson LJ, Ashby MF (1980) Cellular solids structure and properties, Cambridge University Press, Cambridge, England

Hisada T (1995) Recent progress in nonlinear fem-based sensitivity analysis. JSME Int J 38:301–310

Ihara H, Azegami H, Shimoda M (1999) Solution to shape optimization problems considering material nonlinearity. Comput Aided Opt Des Struct 40:87–95

Iwai T, Sugimoto A, Aoyama T, Azegami H (2010) Shape optimization problem of elastic bodies for controlling contact pressure. JSIAM Lett 2:1–4

Kaneko I, Majer G (1981) Optimal design of plastic structures under displacement constraints. Comput Methods Appl Mech Engrg 27:369–391

Kim NH, Choi KK, Chen JS (2000) Shape design sensitivity analysis and optimization of elasto-plasticity with frictional contact. AIAA J 398:1742–1753

Matheson GO, Clement DB, Makenzie DC, Taunton J, Lioyd-Smith D, Maclntyre JG (1987) Stress fractures in athletes: A study of 320 cases. Am J Sports Med 15:46–68

Mills NJ (2007) Polymer foams handbook. Butterworth-Heinemann, Oxford

Nakabe N, Nishiwaki T (2002) Development of simplified numerical foot model for sole stability design. Eng Sport 4:824–830

Nigg BM (1980) Biomechanics of running shoes. Human Kinetics, Champaign, Illinois

Nigg BM, Bahlsen HA, Luethi SM, Stokes S (1987) The influence of running velocity and midsole hardness on external impact forces in heel-toe running. J Biomech 20:951–959

Nigg BM, Herzog W, Read LJ (1988) Effect of viscoelastic shoe insoles on vertical impact forces in heel-toe running. Am J Sports Med 16:70–76

Nishiwaki T (2008) Running shoe sole stiffness evaluation method based on eigen vibration analysis. Sports Technol 1:76–82

Oriwol D, Sterzing T, Milani TL (2011) The position of medial dual density midsole elements in running shoes does not influence biomechanical variables. Footwear Sci 3:107–116

Ryu YS, Haririan M, Wu CC, Arora JS (1985) Structural design sensitivity analysis of nonlinear response. Comput Struct 21:245–255

Stacoff A, Reinschmidt C, Stüssi E (1992) The movement of the heel within a running shoe. Med Sci Sports Exerc 24:695–701

Tanaka M, Noguchi H (2004) Structural shape optimization of hyperelastic material by discrete force method. Theor Appl Mech Japan 53:83–91

Tsay JJ, Arora JS (1990) Nonlinear structural design sensitivity analysis for path dependent problems, part1: General theory. Comput Methods Appl Mech Engrg 81:183–208

Vidal CA, Haber RB (1993) Design sensitivity analysis for rate-independent elastoplasticity. Comput Methods Appl Mech Engrg 107:393–431

Vidal CA, Lee HS, Haber RB (1991) The consistent tangent operator for design sensitivity analysis of history-dependent response. Comput Syst Engrg 2:509–523

Woensel WV, Cavanagh PR (1992) A perturbation study of lower extremity motion during running. Int J Sport Biomech 8:30–47

Yamazaki K, Shibuya K (1998) Sensitivity analysis of nonlinear material and its application to shape optimization. In: Collect Tech Pap AIAA/ASME/ASCE/AHS/ASC Struct Struct Dyn Mater Conf, pp 1706–1713

Yuge K, Kikuchi N (1995) Optimization of a frame structure subjected to a plastic deformation. Struct Optim 10:197–208